

A Real-time Monitoring Technique for Local Plasticity in Metals Based on Lamb Waves and a Directional Actuator/Sensor Set

Y. L. Liu¹, N. Hu², H. Xu³, H. Ning¹ and L. K. Wu¹

Abstract: A real-time monitoring technique for local plasticity using Lamb waves was developed. Tensile test of a thin aluminum plate with a circular hole where high stress concentration was induced was conducted to verify this technique. During the tensile test, a series of wave signals passing through the local plastic region were collected using a directional actuator/sensor set to monitor plasticity evolution. A pulse compression technique was used to process the wave signals. With the increase of tensile stress in the specimen, the amplitude changes of S_0 and A_0 modes were obtained and the difference of Lamb wave signals was further evaluated using a proposed signal index I calculated by wavelet analysis. Combined with the numerical stress analysis of the tensile specimen, the influence of the plasticity on the amplitudes of S_0 and A_0 wave modes was analyzed. As the plastic zone grows gradually, the wave amplitudes and I of S_0 and A_0 wave modes show their different change tendencies compared with those in elastic stage. The amplitude change is more sensitive to mild plasticity than that of I , while the change of I caused by severe plasticity is more obvious than the amplitude change.

Keywords: Lamb waves, local plasticity, pulse compression technique, wavelet analysis.

1 Introduction

Structural health monitoring (SHM) plays an increasingly important role in guarantee of structural safety in recent years [Farrar and Worden (2007); Kulkarni and Achenbach (2008); Nagarajaiah et al. (2009); Yi et al. (2012); Zhang et al. (2012)]. To date, the majority of the research on SHM has been focused on detecting pre-existing visible or relatively large-sized damages such as cracks [Hu et al. (2008);

¹ Department of Mechanical Engineering, Chiba University, Chiba, Japan.

² College of Aerospace Engineering, Chongqing University, Chongqing, China.

³ Mechanical and Electrical Engineering Institute, Beijing University of Chemical Technology, Beijing 100029, China.

Maslouhi (2011); Cho and Lissenden (2012)], holes [Kessler, Spearing and Soutis (2002); Hu et al. (2012)], delamination [Zou, Tong and Steven (2000); Yan and Yam (2004); Hu et al. (2008)], etc. On the other hand, the detection of plastic deformation in the early stage of damage is of paramount importance in engineering application of SHM, as the finally resulted fracture accompanied by crack propagation could lead to serious consequences. For instance, for most of metallic structural components subjected to cyclic loads, fatigue failure scenario usually consists of a crack initiation period and a crack growth period [Ritchie (1999); Chan (2003)]. The crack initiation period is supposed to include the formation and growth of some microcracks which are still too small to be visible. In the subsequent crack growth period, the microcracks merge together gradually to form the main short fatigue cracks which grow comparatively quickly until the complete failure.

Many microscopic investigations have shown that the initiation of invisible microcracks generally occurs very early in the fatigue life. The formation of the microcracks may be resulted by different reasons. For instance, at a fatigue cyclic stress lower than the yield strength, surface grains of materials are less constrained by neighboring grains and therefore easy to slip. As a consequence, microplasticity preferably occurs in grains at the material surface even at a lower stress, which finally leads to the formation of microcracks [Truong, Hirakata and Kitamura (2006)]. Also, the stress higher than yield strength resulted by stress concentration may appear in many structural components because of various reasons, such as the discontinuity of materials geometric irregularity, etc. This will result in local plastic deformation and consequent occurrence of microcracks.

Local plastic zone is considered as a dangerous position of structures, which makes its detection in earlier stage crucial for evaluating the residual life of the structures and preventing possible disasters. At present, there are few methods for detecting the local plasticity, such as chemical corrosion method [France Jr (1970)], electronic speckle pattern interferometry [Gong and Toyooka (1999); Toyooka et al. (2001)], electron backscatter diffraction [Kamaya, Wilkinson and Titchmarsh (2005); Kamaya (2009)]. However, those methods are limited to specific materials and require pre-treatment for specimens. Furthermore, the literatures [Nagy (1998); Herrmann et al. (2006)] reported that nonlinear Rayleigh surface waves and nonlinear ultrasonic bulk waves were applied to the detection of material nonlinearity as an indicator of plasticity-driven damage, and the nonlinear parameters accumulated with wave propagating distance significantly increased when a plate-type intact specimen was under an increasing tensile stress above the yield stress or fatigued with increasing number of cyclic loading. These inspiring results were obtained for a very large plastic area in the specimen, and the sensitivity of the

nonlinear parameters for the local plastic deformation needs further investigations. In addition, the nonlinear wave generation technique is very complex, which requires specific instrumentation, and especially, adjustment of excitation frequency for nonlinear Lamb waves. All of these points make the nonlinear wave techniques difficult to field inspection applications at the present stage.

Therefore, the effort on detecting local plasticity in the early stage of damage or some invisible defects is far from enough. This paper has put forward a real-time monitoring technique for local plasticity using linear Lamb waves, especially fundamental Lamb modes (S_0 and A_0 modes). This technique is based on a hypothesis: supposing that the interaction of Lamb waves with a plastic zone is different from that of Lamb waves with an elastic zone. By investigating the characteristics of S_0 and A_0 modes propagating in an aluminum plate with a circular hole under axial tensile loading, the appearance of local plasticity around the hole can be monitored. In Section 2, an experimental scheme based on a directional actuator/sensor set was designed to demonstrate how the local plasticity could be detected using S_0 and A_0 modes. The experimental data were processed using a pulse compression technique for easily distinguishing the wave signals of S_0 and A_0 modes. The changes of wave amplitude with the increase of stress for both S_0 and A_0 modes were presented to monitor the appearance of the plasticity. Moreover, the obtained wave signals at different stress levels were analyzed through wavelet analysis by virtue of a signal index I , whose variations caused by plastic deformation were more obvious. In Section 3 a series of numerical stress simulations of tensile test were conducted using the finite element analysis (FEA) to further understand the experimental results. Finally, some conclusions were drawn in Section 4.

2 Experiment and results

A thin plate specimen with a circular hole, made from A5052 aluminum with material properties listed in Table 1, was used. The dimensions and geometries of the specimen are shown in Figure 1.

Table 1: Material properties of A5052 aluminum.

Density	Young's modulus	Poisson's ratio	Yield strength	Tensile strength
2710 [kg/m ³]	68.9 [GPa]	0.3	210 [MPa]	260 [MPa]

2.1 Measurement of stress-strain curve

As a pre-requisite, the yielding property of the specimen should be clarified. By using an Instron universal testing machine (Instron 5982, Instron Co.) a preliminary tensile test of the specimen was performed. A strain gauge was attached on the specimen at the position of 5 mm away from the hole (see Figure 1) to measure the strain. For reference, another intact plate specimen with the same size but without a hole was also tested. The obtained nominal stress-nominal strain curves are shown in Figure 2. The yield strength is defined at the stress level corresponding to the intersection of the stress-strain curve with a line parallel to the elastic slope of the curve with an offset of 0.2% strain. It can be seen from Figure 2 that the yield strength is 155 MPa for the specimen with a hole and plasticity occurs in the position where the strain gauge was attached. On the other hand, at the same stress level, the same position for the intact specimen is still in elastic state. Such distinctive difference of these two specimens can be attributed to the high stress concentration around the hole

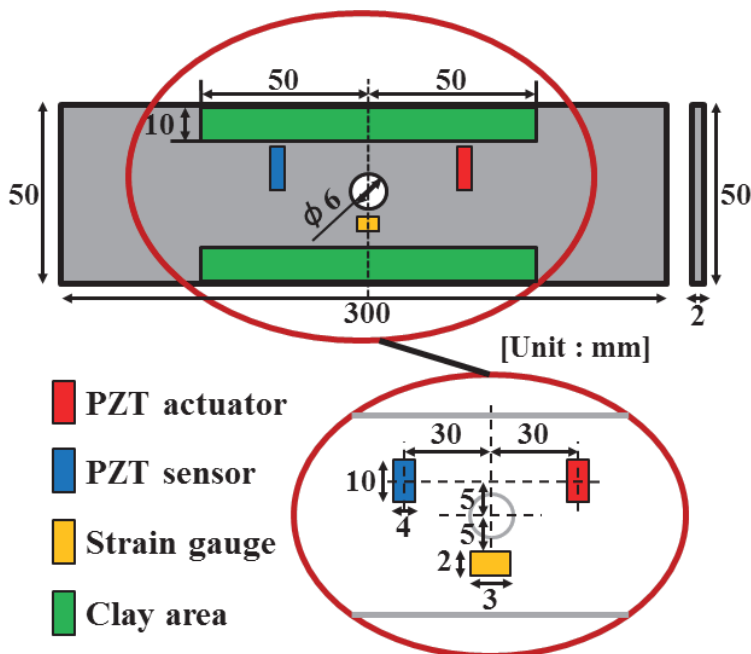


Figure 1: Schematic view of experimental specimen.

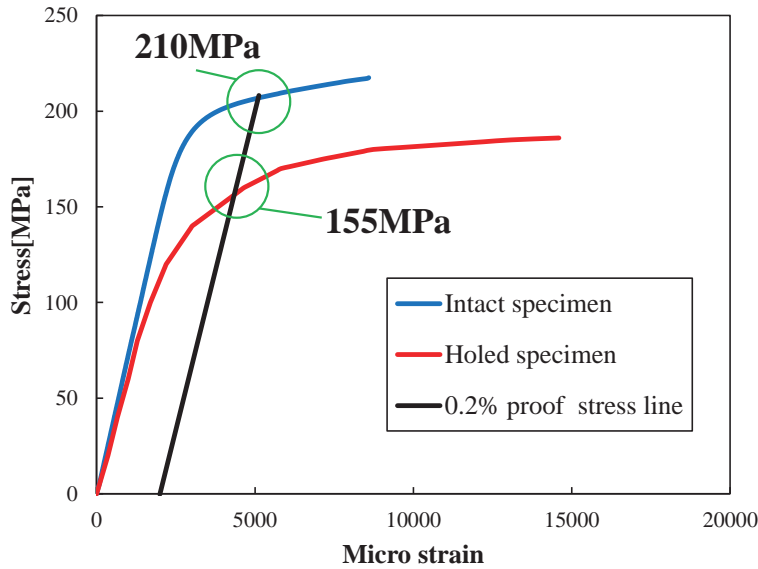


Figure 2: Nominal stress-nominal strain curves.

2.2 Employment of clay and directional actuator/sensor set

For the plate specimen with small sizes as shown in Figure 1, during propagation, Lamb waves will reflect from the four edges of the specimen within a short time. It can be predicted that these reflections will be mixed with the target wave signals, which increases the complexity of wave signal analysis. To reduce the reflections from boundaries, we employed two methods. First, we laid fat clay of the thickness of 5 mm on the two sides of the plate (see Figure 1, front and back surfaces of the plate). It is well-known that acoustic impedance of the fat clay is much closer to that of the aluminum compared to air, thus the reflections from the two side boundaries might be decreased. The experimental data demonstrated that the fat clay can effectively reduce the reflection intensity from the two sides of the plate. Second, a directional actuator/sensor set was designed to concentrate wave energy in wave propagation direction as much as possible. As well-known, a circular-type lead zirconate titanate (PZT) actuator or sensor can generate or receive waves uniformly in all directions, which is not suitable for the present plate specimen with small sizes. Therefore, rectangular-type PZTs were employed in the present research.

Two verification experiments were conducted to study the directionality of rectangular-type PZTs. The experiment as shown in Figure 3 was performed to inves-

tigate the characteristics of generated S_0 and A_0 modes in different directions and different distances when a rectangular-type PZT (width 10mm, thickness 0.5mm, length 4mm, FUJI Ceramics Co.) with around 200kHz resonant frequency was used as actuator and an acoustic emission (AE) sensor (AE-930N, Electronic Instrument Co.) was used. Moreover, in this research, the chirp burst wave was chosen as the input signal on the actuator, which can be described as follows:

$$P(t) = \begin{cases} [0.5 - 0.5 \cos(\frac{2\pi t}{T})] \sin[2\pi(f_0 t + \frac{B}{2T} t^2)] & t \leq T \\ 0 & t > T \end{cases} \quad (1)$$

where t is time in second, f is the central frequency and B is the frequency sweep width. In this experiment, $f=40$ kHz, $B= f/2$ kHz, $T=(1/f) \times 5000$ sec. Figure 4 shows the waveform in time domain and the frequency spectrum of the input signal. From it, we can see that the incident wave is a broad-band signal in frequency domain from 0 to 80 kHz. By virtue of dispersion curves of group velocity for an aluminum plate shown in Figure 5, it can be predicted that only S_0 and A_0 modes can be generated in the thin plate specimen.

The amplitudes of S and A modes generated by the rectangular-type PZT actuator in different directions were compared in Figure 6, and the result of a circular PZT actuator (diameter 10mm, thickness 0.5mm, FUJI Ceramics Co.) at 0° direction was also plotted (see Figure 6, "Normal"). It can be seen from Figures 6(a) and 6(b) that the amplitudes of both S_0 and A_0 mode at 0° direction are much larger than those of other directions using the rectangular-type PZT actuator and the circular-type PZT actuator in 0° direction. It implies that the rectangular-type PZT actuator can effectively concentrate the wave energy in the wave propagation direction, and reduce those wave energies in other directions, leading to the weak reflections of boundaries.

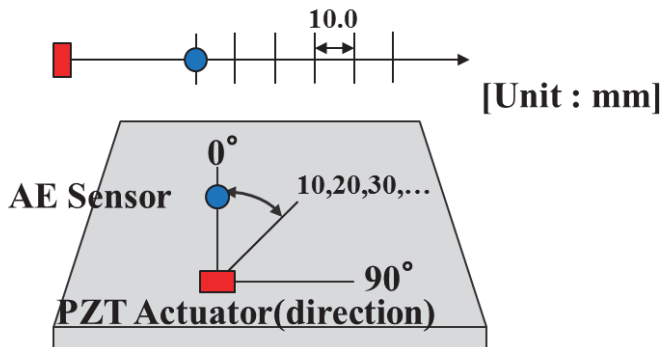


Figure 3: Schematic view of experiment (rectangular-type PZT used as actuator).

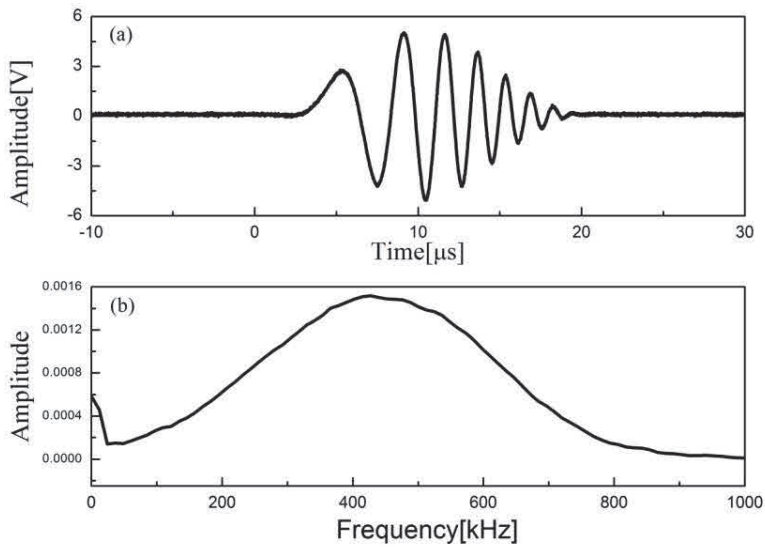


Figure 4: Input signal: (a) waveform in time domain and (b) FFT spectrum.

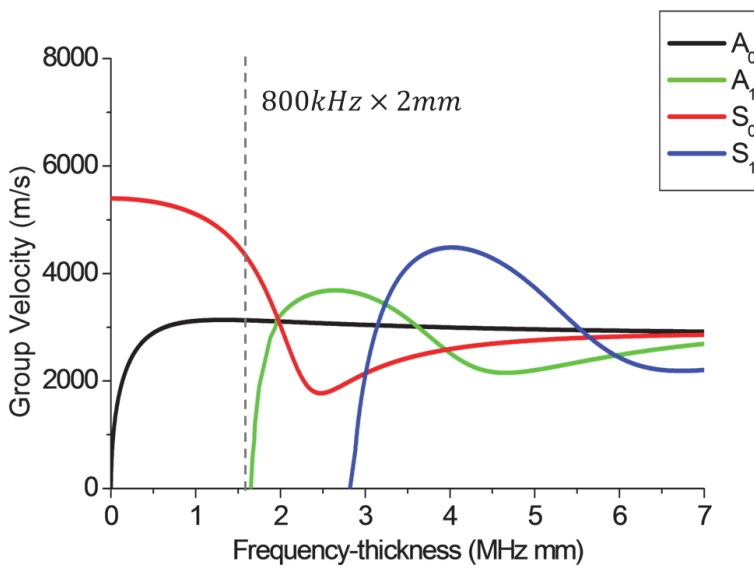


Figure 5: Dispersion curves of group velocity for an aluminum plate.

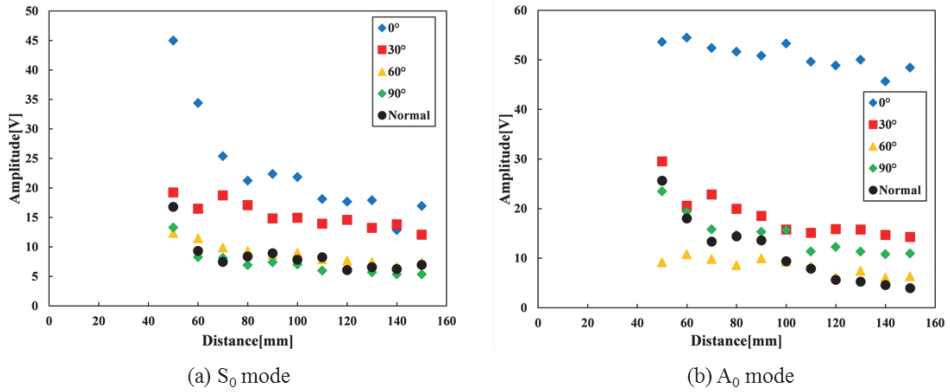


Figure 6: Amplitudes of generated Lamb waves in different directions: (a) S_0 mode and (b) A_0 mode.

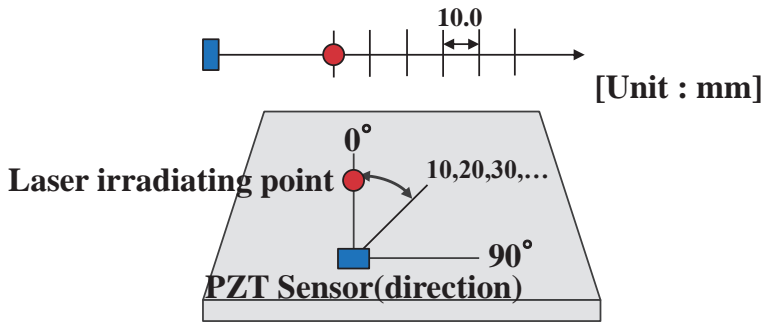


Figure 7: Schematic view of experiment (rectangular-type PZT used as sensor).

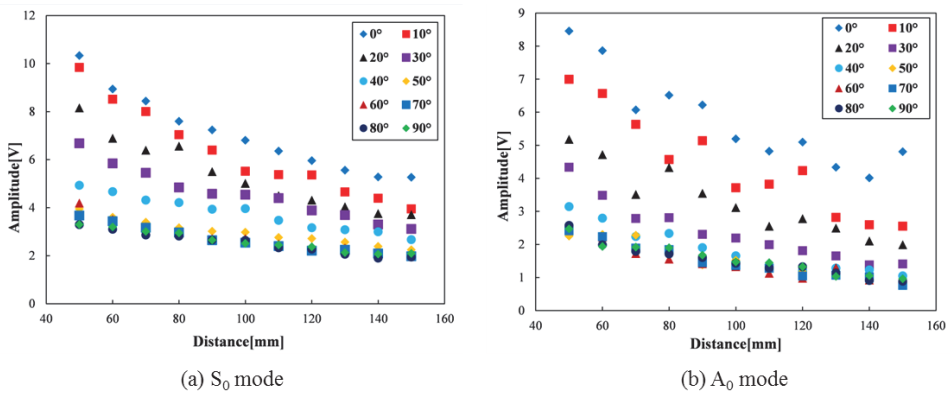


Figure 8: Amplitudes of received Lamb waves in different directions: (a) S_0 mode and (b) A_0 mode

When a rectangular-type PZT was used as sensor, and pulse laser irradiation was used as actuator, another experiment as shown in Figure 7 was carried out to investigate the sensor sensitivity when receiving S_0 and A_0 modes in different directions and different distances. The amplitudes of S_0 and A_0 modes received by the rectangular-type PZT sensor in different directions were compared in Figure 8. It can be seen that the rectangular-type PZT is much more sensitive to S_0 and A_0 Lamb waves at 0° direction than other directions. Therefore, it can mainly receive the wave energy in the wave propagation direction, and effectively avoid the mixing of other unnecessary reflections from boundaries. In the present study, a directional actuator/sensor set (see Figure 1) made from rectangular-type PZTs was employed.

2.3 Description of experimental scheme

Based on the above results, an experimental scheme was designed to monitor the change of wave signals during the tensile test, especially at the transition stage from elastic state to plastic state. The corresponding specimen and experimental setup are schematically shown in Figures 1 and 9. A thin aluminum plate specimen with a circular hole was gradually stretched to the nominal stress of 190MPa, which was much higher than the previously measured yield stress, i.e., 155MPa. At the same time, for every stress increment of 1/3 MPa, Lamb waves were generated and received using the directional PZT actuator/sensor set bonded on the surfaces of the specimen (see Figure 1). The wave signals propagating along the straight path between the actuator and the sensor (see Figure 9) were recorded corresponding to different stress levels.

Because of the narrow width of specimen, the target waves might be easily mixed with the reflections from the specimen boundaries, leading to more difficult analysis of wave signals. For this reason, the previously stated fat clay and directional actuator/sensor set with rectangular-type PZTs (see Figure 1), were used to increase wave intensity along the straight path between actuator and sensor and suppress the wave intensities from other directions.

2.4 Experimental results

Figure 10(a) illustrates the original waveforms at different stress levels obtained by the sensor during the tensile test. The first wave packet is S_0 mode and the second wave packet is A_0 mode. It can be seen that the two wave packets are slightly overlapped and the difference of those wave signals at different tensile loads are very small. To separate the S_0 and A_0 wave packets and amplify the difference of the wave signals at different stress levels, a pulse compression technique was used.

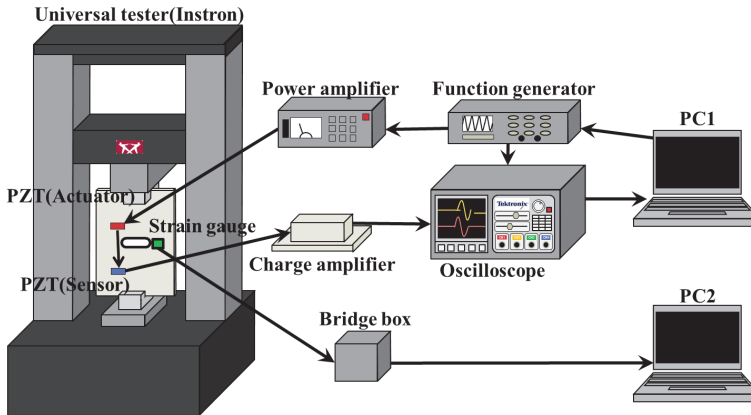


Figure 9: Experimental setup.

It can be expressed in the following equation:

$$C(t) = \int R(\tau)ref(t + \tau)d\tau \quad (2)$$

where $R(t)$ is a received signal and $ref(t)$ is a reference signal. The obtained pulse compression signal $C(t)$ expresses the cross-correlation of the received signal with a reference signal as shown in Figure 11. In general, the excitation signal (i.e., the chirp burst wave in this work) is used as the reference signal. This signal processing technique can compress the pulse width in time domain and increase the signal intensity. Figure 10(b) demonstrates the wave signals processed by the pulse compression technique at different stress levels. It can be seen that the S_0 and A_0 modes are separated clearly and the difference of wave signals at different stress levels becomes more obvious. Thus, the reported following results are based on the processed wave signals by this pulse compression technique. In this case, the meaning of the signal amplitude is different from that of a common PZT sensor signal in the unit of voltage.

Firstly, the amplitude change of S_0 and A_0 modes with the increase of stress level in the specimen was investigated. Figure 12 shows the amplitude variation of S_0 mode. The amplitude of S mode increases slightly with the increase of the tensile load in elastic deformation. However, at around 130MPa, it starts to decrease. At 155MPa, it increases remarkably again. For the case of A_0 mode in Figure 13, unlike that of S_0 wave mode, the amplitude of A_0 mode decreases as the tensile load increases in elastic state. This decrease stops at around 130MPa, corresponding to the lowest amplitude. Then the amplitude starts to increase slowly, and grows

rapidly when the stress level in the specimen reaches 155MPa. Note that, prior to 155 MPa, the variations of the wave amplitudes of both S_0 and A_0 modes in Figures 12 and 13 are very small.

Secondly, the difference of Lamb wave signals related to different loads was evaluated using wavelet analysis. Note that the intact wave signals containing both S_0 and A_0 wave packets were processed. In wavelet analysis, as shown in Figure 14, a signal can be divided into an approximate primary subset (low frequency information, A1) and a detailed subset (high frequency information, D1). A1 can then be further divided into a second-level approximate primary subset (A2) and its detailed subset (D2), and this process can be repeated. In this work, Daubechies wavelet (db10) was used as the mother wavelet. The decomposition level is 3 and the wave signals were decomposed into 4 subsets (A3+D3+D2+D1) in different frequency bands. A signal index I was defined as follows to evaluate the change of wave signals during the tensile test

$$I(\sigma_i) = \sqrt{\frac{\sum_n [w(X_n; \sigma_i) - w_b(X_n; \sigma_b)]^2}{\sum_n [w_b(X_n; \sigma_b)]^2}} \quad (3)$$

where X is one of the decomposed subsets (A3, D3, D2, D1), n is the number of sampling data, w is the n th number of the decomposed parameter X of subset at the stress σ_i , and $w_b(X_n; \sigma_b)$ is the corresponding baseline signal recorded at the stress level of σ_b . Here, the wave signal obtained in the unloaded specimen was used as the baseline signal, i.e., $\sigma_b = 0$. The signal index I of Lamb waves was calculated and shown in Figure 15. It can be seen that the I corresponding to the A3, D3 and D2 subsets present some meaningful and interesting variations, but the I corresponding to the D1 subset are very scattered around a value of 1.35, which is meaningless and may be caused by noises. In Figure 15, all I corresponding to the A3, D3 and D2 subsets increase with the stress level and a sudden increase appears at 160 MPa for the D3 and D2 subsets, while the appearance of a sudden increase in the I of the A3 subset is at 170 MPa (Figure 15(a)). In this case, we can also find that the increasing rate of I increases remarkably from 160 MPa.

3 Discussion

To further understand the above experimental results, a series of numerical simulations were conducted to explore the plasticity evolution around the hole during tensile test by using a commercial FEA software ABAQUS. Here, a two-dimensional (2D) model of a rectangular plate with a circular hole under stretching in plane stress was built up, and its sizes and material parameters are the same with those in the experiment.

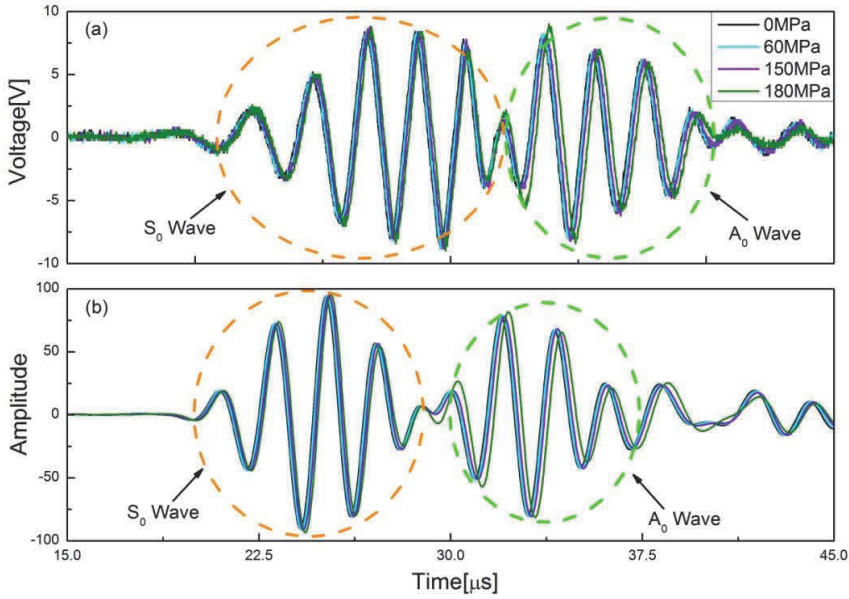


Figure 10: Wave signals: (a) Original wave signals at different stress levels and (b) Wave signals processed by pulse compression technique at different stress levels.

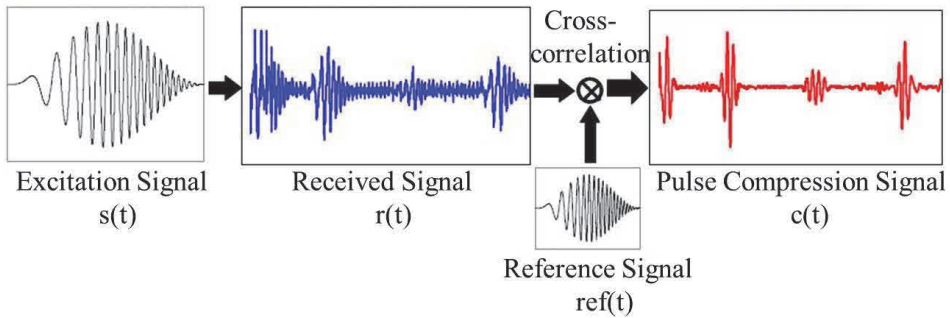


Figure 11: Pulse compression technique.

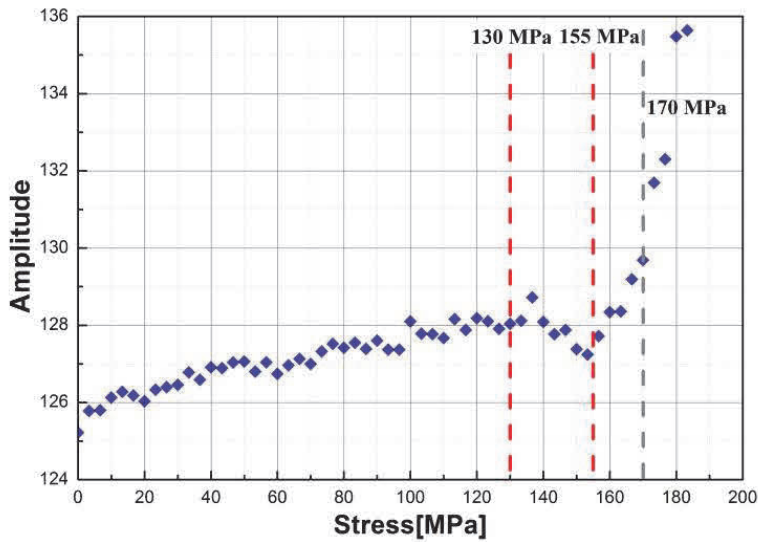


Figure 12: Amplitude change of S_0 Lamb mode with the increase of stress level in the specimen.

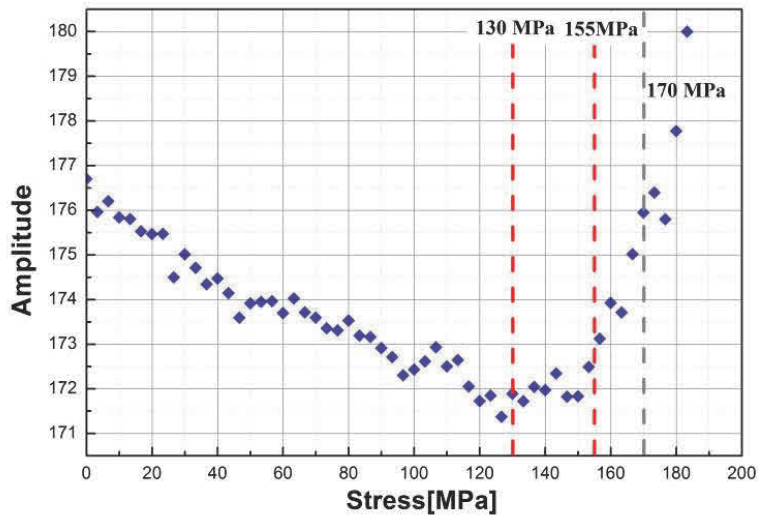


Figure 13: Amplitude change of A_0 Lamb mode with the increase of stress level in the specimen.

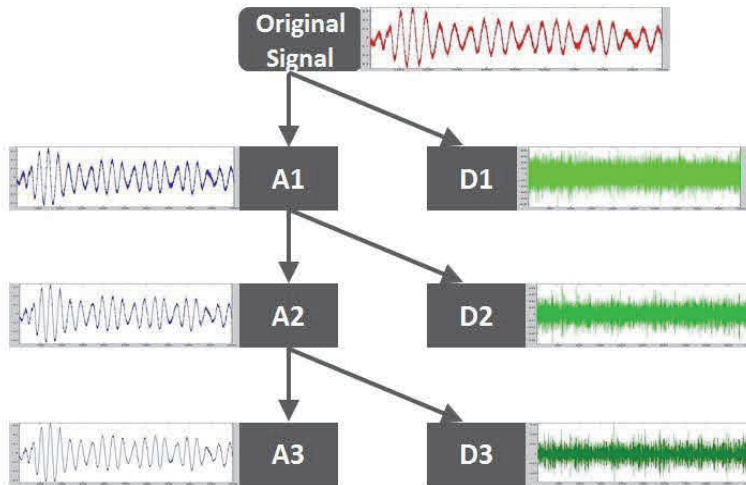
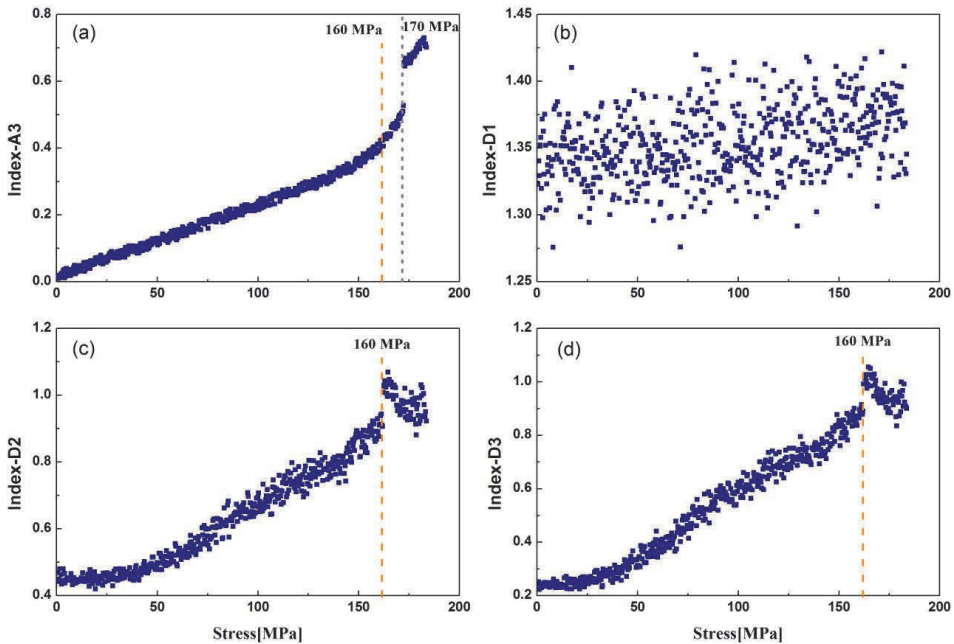


Figure 14: Wavelet analysis of signals.

Figure 15: Signal index I related to different stress levels: (a) A3, (b) D1, (c) D2 and (d) D3

The evolution of plastic zone around the hole at the stress levels from 75MPa to 180MPa is shown in Figure 16. The plastic zone is represented by dark grey color. When the stress in the specimen reaches 75MPa, two small plastic zones initially appear at both sides of the hole (Figure 16(a)). With the increase of the applied stress, they gradually become larger (Figure 16(b)). Figure 16(c) shows the plastic state when the stress is up to 155MPa. At this stage, the position of the strain gauge goes into plastic state. As the applied stress continues increasing, plastic zones extend towards to the direction at the angle of $\pm 45^\circ$ (Figures 16(d) and 16(e)) due to shear banding, and the size of plastic zones grows rapidly when the stress increases from 170 MPa to 180 MPa (Figure 16(f)).

For convenience of discussion, the above process can be categorized into three stress stages: (1) 0MPa~130MPa, (2) 130MPa~155MPa, (3) 155MPa~180MPa.

3.1 0MPa~130MPa

At this stage, the amplitude variation tendency of S_0 wave mode is opposite to that of A_0 mode (see Figures 12 and 13). For a particle-spring model as shown in Figure 17, it is well-known that in S_0 wave mode, particles vibrate along the wave propagation direction, meanwhile, in A_0 wave mode particles vibrate along the normal direction or plate thickness direction. Since the applied axial stress direction in the specimen is the same with that of particle movement in S_0 wave mode, this may promote the propagation of S_0 wave mode and amplify its amplitude (see Figure 12). On the other hand, since the applied axial stress is vertical to the particle movement direction in A_0 wave mode the propagation of A_0 wave mode may be restrained by the axial stress (see Figure 13). This is just similar to the case where the transverse vibration amplitude of a spring can be suppressed by stretching the spring. In addition, the linear increase of the I corresponding to the A3, D3 and D2 subsets also clearly indicates that the influence of the increase of stress levels on Lamb wave propagation is stable.

From numerical results in Figure 16, we can see that the plasticity occurs initially when the stress is up to 75MPa. However, at this stress level or even up to 130MPa, we cannot identify any obvious change in either amplitude or I which means that linear Lamb waves (S and A wave modes) are insensitive to the initial plastic deformation. At this stage, the plastic zone is too small to affect the wave propagation (Figures 16(a) and 16(b)).

3.2 130MPa~155MPa

At this stage, unlike the previous stress stage, the amplitude of S wave mode decreases gradually (see Figure 12) while the amplitude of A wave mode increases (see Figure 13). These changes may be due to the softening caused by plastici-

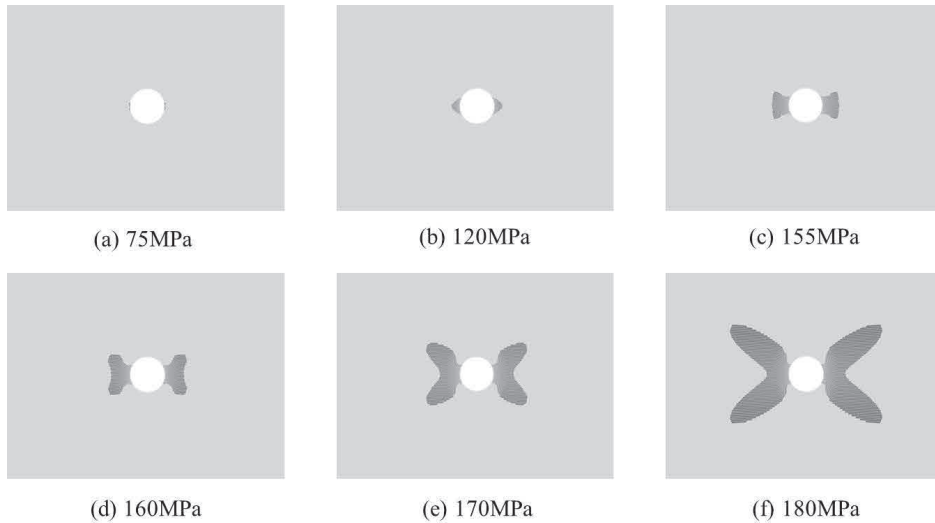


Figure 16: Evolution of plastic zone during loading process: (a) 75 MPa, (b) 120 MPa, (c) 155 MPa, (d) 160 MPa, (e) 170 MPa and (f) 180 MPa.

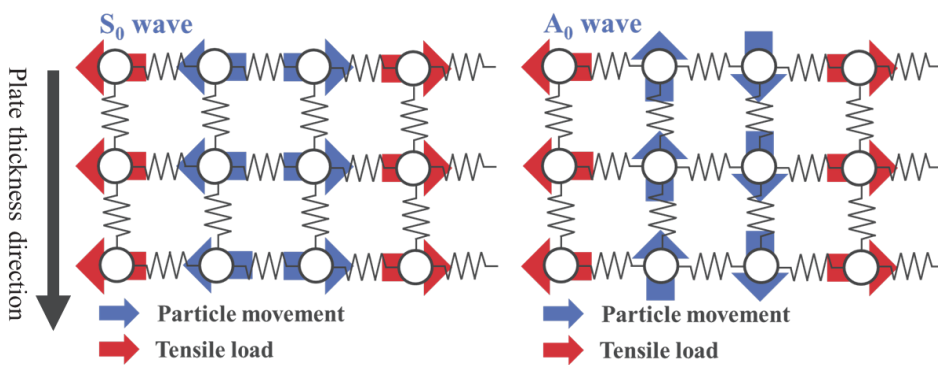


Figure 17: Lamb wave propagation model (one dimension).

ty evolution. At end of this stage (i.e., 155MPa), the plastic zone extends to the position of 5 mm away from the hole as shown in Figure 1 and Figure 16(c). Although the plastic zone is still small, it already starts to influence the amplitude of wave signals, which means the plasticity can be firstly discovered by the amplitude change of wave signals. However, the change tendency of I is not obvious at this stage (see Figure 15). Therefore, the change of wave amplitude is more sensitive to mild plastic deformation than that of I .

3.3 155MPa~180MPa

At the starting point of this stage, i.e., 155 MPa, both wave amplitudes of S_0 and A_0 modes increase remarkably (see Figures 12 and 13), implying the significant softening of material or springs in Figure 17 caused by severe plasticity. However, the absolute increases of the wave amplitudes are small by observing the values on the longitudinal axe of Figures 12 and 13. Moreover, the sudden increases of I for the D3 and D2 subsets at 160 MPa can be identified from Figures 15(c) and 15(d), which are caused by the extension of plastic zone. At the same stress level, the increasing rate of I corresponding to the A3 subset begins to increase slightly in Figure 15(a). Therefore, the detailed subsets (i.e., D3 and D2) are more sensitive to plasticity than the approximate primary subset (i.e., A3 subset). As the load keeps on going, a sudden increase of the I for the A3 subset also appears at 170 MPa. Besides, the amplitudes of both S_0 and A_0 wave modes in Figures 12 and 13 increase more rapidly from 170 MPa. This phenomenon may be caused by the geometry change of the hole in severe plasticity. In this case, because the circular profile of the hole changes into elliptic one with its major axis parallel to the wave propagation direction, the waves can transmit through the hole area more easily. Moreover, compared with the absolute changes of wave amplitudes in Figures 12 and 13, the absolute changes of I are much higher in Figure 15, indicating that I is more suitable for monitoring the severe plasticity.

4 Conclusions

In this work, we developed a real-time monitoring technique for local plasticity using linear Lamb waves. To verify the effectiveness of the proposed technique, tensile test of a thin plate specimen with a circular hole was conducted. Stress concentration was generated around the hole, leading to local plasticity. Two rectangular-type commercial PZTs attached on the specimen were used as a directional actuator/sensor set to collect strong and clear wave signals during the tensile test. The path between the actuator and the sensor was chosen to monitor the appearance of the local plasticity. Wave signals corresponding to different tensile stress were processed using a pulse compression technique. The amplitude changes of S_0 and A_0

wave modes with the increase of the tensile stress in the specimen were investigated and a signal index I based on wavelet analysis was defined to study the difference of Lamb wave signals caused by plasticity. To further understand the experimental results, a series of FEA numerical simulations of the tensile test were conducted to explore the plasticity evolution process around the hole. Base on the experimental and numerical results, it can be found that both S_0 and A_0 wave modes are insensitive to the appearance of initial plasticity. As the plastic zone gradually extends larger, the amplitudes of S_0 and A_0 wave modes show their different change tendencies compared with those in elastic stage. It is also found that the amplitude change is more sensitive to mild plasticity than the change of I , while the change of I caused by severe plasticity is more obvious than the amplitude change. Therefore, the proposed technique can effectively monitor the evolution of plasticity.

References

- Chan, K. S.** (2003): A Microstructure-Based Fatigue-Crack-Initiation Model. *Metall Mater. Trans A*, vol. 34, pp. 43-58.
- Cho, H.; Lissenden, C. J.** (2012): Structural Health Monitoring of Fatigue Crack Growth in Plate Structures with Ultrasonic Guided Waves. *Struct Health Monit*, vol. 11, pp. 393-404.
- Farrar, C. R.; Worden, K.** (2007): An Introduction to Structural Health Monitoring. *Philos. Trans R Soc. London, Ser. A*, vol. 365, pp. 303-315.
- France, Jr, W.** (1970): Effects of Stress and Plastic Deformation on the Corrosion of Steel. *Corrosion*, vol. 26, pp. 189-199.
- Gong, X.; Toyooka, S.** (1999): Investigation on Mechanism of Plastic Deformation by Digital Speckle Pattern Interferometry. *Exp Mech*, vol. 39, pp. 25-29.
- Herrmann, J.; Kim, J.-Y.; Jacobs, L. J.; Qu, J.; Littles, J. W.; Savage, M. F.** (2006): Assessment of Material Damage in a Nickel-Base Superalloy Using Nonlinear Rayleigh Surface Waves. *J. Appl Phys*, vol. 99, pp. 124913.
- Hu, N.; Cai, Y.; Zhu, G.; Tsuji, C.; Liu, Y.; Cao, Y.** (2012): Characterization of Damage Size in Metallic Plates Using Lamb Waves. *Struct Health Monit*, vol. 11, pp. 125-137.
- Hu, N.; Shimomukai, T.; Fukunaga, H.; Su, Z.** (2008): Damage Identification of Metallic Structures Using A_0 Mode of Lamb Waves. *Struct Health Monit*, vol. 7, pp. 271-285.
- Hu, N.; Shimomukai, T.; Yan, C.; Fukunaga, H.** (2008): Identification of Delamination Position in Cross-Ply Laminated Composite Beams Using S_0 Lamb Mode. *Compos. Sci. Tech.*, vol. 68, pp. 1548-1554.

Kamaya, M. (2009): Measurement of Local Plastic Strain Distribution of Stainless Steel by Electron Backscatter Diffraction. *Mater Charact*, vol. 60, pp. 125-132.

Kamaya, M.; Wilkinson, A. J.; Titchmarsh, J. M. (2005): Measurement of Plastic Strain of Polycrystalline Material by Electron Backscatter Diffraction. *Nucl Eng Des*, vol. 235, pp. 713-725.

Kessler, S. S.; Spearing, S. M.; Soutis, C. (2002): Damage Detection in Composite Materials Using Lamb Wave Methods. *Smart Mater Struct*, vol. 11, pp. 269.

Kulkarni, S.; Achenbach, J. (2008): Structural Health Monitoring and Damage Prognosis in Fatigue. *Struct Health Monit*, vol. 7, pp. 37-49.

Maslouhi, A. (2011): Fatigue Crack Growth Monitoring in Aluminum Using Acoustic Emission and Acousto-Ultrasonic Methods. *Struct Control Health Monit*, vol. 18, pp. 790-806.

Nagarajaiah, S.; Dyke, S.; Lynch, J.; Smyth, A.; Agrawal, A.; Symans, M.; Johnson, E. (2009): Current Directions of Structural Health Monitoring and Control in USA. *Advances in Science and Technology*, vol. 56, pp. 277-286.

Nagy, P. B. (1998): Fatigue Damage Assessment by Nonlinear Ultrasonic Materials Characterization. *Ultrasonics*, vol. 36, pp. 375-381.

Ritchie, R. O. (1999): Mechanisms of Fatigue-Crack Propagation in Ductile and Brittle Solids. *Int J. Fracture*, vol. 100, pp. 55-83.

Toyooka, S.; Widiastuti, R.; Zhang, Q. and Kato, H. (2001): Dynamic Observation of Localized Strain Pulsation Generated in the Plastic Deformation Process by Electronic Speckle Pattern Interferometry. *Jpn. J Appl Phys*, vol. 40, pp. 873.

Truong, D. V.; Hirakata, H.; Kitamura, T. (2006): Effect of Loading Frequency on Fatigue Crack Growth between a Submicron-Thick Film and a Substrate. *JSME Int J A-Solid M.*, vol. 49, pp. 370-375.

Yan, Y.; Yam, L. (2004): Detection of Delamination Damage in Composite Plates Using Energy Spectrum of Structural Dynamic Responses Decomposed by Wavelet Analysis. *Comput. & Struct.*, vol. 82, pp. 347-358.

Yi, J.-H.; Kim, D.; Go, S.; Kim, J.-T.; Park, J.-H.; Feng, M.Q. and Kang, K.-S. (2012): Application of Structural Health Monitoring System for Reliable Seismic Performance Evaluation of Infrastructures. *Adv Struct. Eng*, vol. 15, pp. 955-968.

Zhang, D.; Bao, Y.; Li, H.; Ou, J. (2012): Investigation of Temperature Effects on Modal Parameters of the China National Aquatics Center. *Adv Struct. Eng*, vol. 15, pp. 1139-1154.

Zou, Y.; Tong, L.; Steven, G. (2000): Vibration-Based Model-Dependent Damage (Delamination) Identification and Health Monitoring for Composite Structures—a

Review. *J Sound Vib*, vol. 230, pp. 357-378.

